AIAA JOURNAL
Vol. 47, No. 11, November 2009

Noise Source Localization and Optimization of Phased-Array Results

Patricio A. Ravetta*
AVEC, Inc., Blacksburg, Virginia 24060
and
Ricardo A. Burdisso† and Wing F. Ng‡
Virginia Polytechnic Institute and State University, Blacksburg, Virginia 24061

DOI: 10.2514/1.38073

A new approach to the deconvolution of acoustic sources has been developed and is presented in this work. The goal of this postprocessing is to simplify the beamforming output by suppressing the side lobes and reducing the sources' main lobes to single (or a small number of) points that accurately identify the noise sources' positions and their actual levels. In this work, a new modeling technique for the beamforming output is proposed. The idea is to use an image-processing-like approach to identify the noise sources from the beamforming maps: that is, recognizing lobe patterns in the beamformed output and relating them to the noise sources that would produce that map. For incoherent sources, the beamforming output is modeled as a superposition of point-spread functions and a linear system is posted. For coherent sources, the beamforming output is modeled as a superposition of complex point-spread functions and a nonlinear system of equations in terms of the sources' amplitudes is posted. As a first approach to solving this difficult problem, the system is solved using a new two-step procedure. In the first step, an approximated linear problem is solved. In the second step, an optimization is performed over the nonzero values obtained in the previous step. The solution to this system of equations renders the sources' positions and amplitudes. In the case of coherent sources, their relative phase can also be recovered. The technique is referred as noise source localization and optimization of phased-array results. A detailed analytical formulation, numerical simulations, and sample experimental results are shown for the proposed postprocessing.

Nomenclature

$a(\mathbf{x}'')$	=	source strength for a source at $\mathbf{x}''$
$b(\mathbf{x})$	=	beamforming output power at the point $\mathbf{x}$
$b_R(\mathbf{x}_i)$	=	reconstructed beamforming output at the point $\mathbf{x}_i$
$b'(\mathbf{x})$	=	linear approximation to the actual beamforming output $b(\mathbf{x})$ at the point $\mathbf{x}$
C	=	correlation coefficient
$C_j(\mathbf{x}')$	=	complex array response for microphone j for a source at $\mathbf{x}'$
$\mathrm{cpsf}(\mathbf{x}, \mathbf{x}'')$	=	complex point-spread function at the point $\mathbf{x}$ for a source at $\mathbf{x}''$
$\hat{\mathbf{E}}$	=	matrix of complex point-spread functions
$f(\mathbf{b}, \mathbf{a})$	=	error function
J	=	total number of microphones
K	=	wave number
M	=	actual number of sources
N	=	number of grid points
NZ	=	number of nonzero sources from approximated solution
$\mathbf{p}$	=	vector containing the for each of the array microphones
$\mathrm{psf}(\mathbf{x}, \mathbf{x}'')$	=	point-spread function at the point for a source at $\mathbf{x}''$
p_j	=	frequency-domain pressure at microphone j
$s(\mathbf{x})$	=	source distribution function
$\mathbf{w}(\mathbf{x})$	=	array weighting factor, also known as steering vector
$\mathbf{x}$	=	position vector
$y(\mathbf{x})$	=	complex beamformed pressure at the point
$\delta(\mathbf{x}' - \mathbf{x}'')$	=	Dirac's delta function
ξ_n	=	error between actual and modeled beamforming output for a grid point at $\mathbf{x}_n$
$\langle\,\rangle$	=	time-averaged of short-time Fourier transform signals

Presented as Paper 2713 at the 12th AIAA/CEAS Aeroacoustics Conference (27th AIAA Aeroacoustics Conference), Cambridge, MA, 8–10 May 2006; received 14 April 2008; revision received 21 November 2008; accepted for publication 25 November 2008.

*Chief Research Engineer, 3154 State Street Suite 2230. Senior Member AIAA.
†Professor, Mechanical Engineering Department, Mail Code 0238. Member AIAA.
‡Chris Kraft Endowed Professor, Mechanical Engineering Department, Mail Code 0238. Associate Fellow AIAA.

I. Introduction

DURING the past years, microphones phased-array measurements have become a common practice in aeroacoustic testing. The use of this technology allows creating a sound picture at each frequency of interest showing the most significant noise sources. However, one of the problems with phased-array measurements is that the beamforming maps are usually contaminated by side lobes (i.e., lobes not associated with actual sources). Thus, it could be difficult to clearly identify the noise sources' positions and actual levels from the beamforming maps. This problem is especially true for complex source distributions, for coherent sources, and when some of the sources are at or under the array signal-to-noise ratio (SNR) (i.e., side lobes that can be assumed to be noise sources and vice versa). As a consequence, the interpretation of the beamforming maps has to be performed with care to properly identify the real noise sources, in which case some sources that look like side lobes might be overlooked.

To overcome these issues, a beamforming postprocessing technique called DAMAS (deconvolution approach for the mapping of acoustic sources) was developed by Brooks and Humphreys in 2004 [1]. This technique represented a breakthrough in array processing and led the way for future phased-array analysis. The DAMAS

technique models the cross-spectral matrix (CSM) and obtains an inverse problem in which the power of the noise sources is obtained. Because the CSM is usually ill-conditioned (i.e., noninvertible), a Gauss–Seidel iterative scheme is used to solve for the sources' power. However, as mentioned in the original work, the required computational time and some other restrictions limit the capabilities of this approach. In 2005, Brooks and Humphreys [2] explored the application of DAMAS to three-dimensional cases. In the same year, Dougherty [3] proposed modifications to the DAMAS technique (DAMAS 2 and 3) using regularization techniques that significantly reduce the computational time and also reduce the number of iterations required. These approaches, however, unlike the technique to be presented next, limit the point-spread function to a translationally invariant, convolutional form. A very interesting comparison between different deconvolution techniques can be seen in the work by Ehrenfried and Koop [4] (2006).

Also in 2006, Brooks and Humphreys [5] demonstrated the capability of DAMAS-C to account for coherent sources using cross-beamforming over the source region. However, the size and complexity of the posted problem (i.e., equivalent to solving DAMAS in N grids with N scanning points: thus, on the order of N^2 variables) makes it hard to implement in a practical way. As will be shown in this work, a simpler problem can be posted and solved.

In 2007, Sijtsma [6] introduced CLEAN-SC to account for spatial source coherence and was able to successfully apply the technique to wind-tunnel measurements of airfoil noise. As mentioned in his work, CLEAN-SC has the advantage that, unlike LORE and DAMAS, it is not based on the theoretical point-spread function (psf). This means that results are not affected by test conditions such as reverberant environments and poor array calibration.

In our work, a new postprocessing technique for the beamforming output is proposed. The main idea is to use an image-processing-like approach to identify the noise sources from the beamforming maps. This is achieved by recognizing patterns in the beamformed output and relating them to the noise sources that would produce that map. The technique is referred to here as noise source localization and optimization of array results (LORE). Using this technique, the modeling of the beamforming output is obtained more accurately and unambiguously. The postprocessing results at each frequency are the actual noise sources' positions and levels. Because the technique can also solve for relative phase, coherent sources can also be identified. The use of these results at every frequency of interest also provides the ability to obtain the spectrum of a source without using integration of the maps, thus avoiding some issues related to array integration techniques (e.g., normalization, array size effects, and grid resolution [7]).

The computational time required for LORE to obtain a solution is significantly reduced when compared with DAMAS. Other issues present in the DAMAS approach, such as position of the actual source relative to the scanning grid [3], are not an issue in the new approach (as long as the actual source position is inside the scanning grid). Unlike DAMAS 2 and 3, the theoretical formulation is not restricted to small regions in space and can be applied to 2-D or 3-D cases.

II. Theoretical Formulation

The starting point in the LORE formulation is the source-receiver model. Thus, at microphone j, the time-averaged frequency-domain pressure $\langle p_j \rangle$ can be expressed as the superposition of the sound radiating from a spatial distribution of sources as

$$\langle p_j \rangle = \int C_j(\mathbf{x}')\langle s(\mathbf{x}')\rangle \, \mathrm{d}\mathbf{x}' \tag{1}$$

where $\langle s(\mathbf{x}')\rangle$ is the time-averaged short-time Fourier transform of the amplitude for a source at $\mathbf{x}'$, and $C_j(\mathbf{x}')$ is the complex array response for microphone j, given by the frequency-domain Green's function for a source at $\mathbf{x}'$ in free space as

$$C_j(\mathbf{x}') = \frac{e^{-ik|\mathbf{x}'-\mathbf{x}_j|}}{4\pi|\mathbf{x}'-\mathbf{x}_j|} \tag{2}$$

where $\mathbf{x}_j$ is the position of microphone j, and k is the wave number.

Arranging the signals for all J microphones in a vector $\langle \mathbf{p} \rangle$, the beamforming output power for a grid point at $\mathbf{x}$ can be written as

$$b(\mathbf{x}) = |\mathbf{w}^{\dagger}(\mathbf{x})\langle \mathbf{p} \rangle|^2 \tag{3}$$

where $\mathbf{w}(\mathbf{x})$ is the array weighting factor, also known as the steering vector, given by

$$\mathbf{w}(\mathbf{x}) = \frac{\mathbf{C}(\mathbf{x})}{\|\mathbf{C}(\mathbf{x})\|} \tag{4}$$

Note that the choice for the steering vector is not restricted to the preceding definition. Thus, flow convection and other corrections can be included in its definition to implement the proposed approach.

Replacing Eq. (1) in Eq. (3),

$$b(\mathbf{x}) = \left| \mathbf{w}^{\dagger}(\mathbf{x}) \int \mathbf{C}(\mathbf{x}')\langle s(\mathbf{x}')\rangle \, \mathrm{d}\mathbf{x}' \right|^2 \tag{5}$$

If the simplest source distribution for $\langle s(\mathbf{x}')\rangle$ is assumed [i.e., a single point source at $\mathbf{x}''$, with source strength $a(\mathbf{x}'')$], it can be written as

$$\langle s(\mathbf{x}')\rangle = \langle a(\mathbf{x}'')\rangle \delta(\mathbf{x}' - \mathbf{x}'') \tag{6}$$

Then the beamformed output power at the point $\mathbf{x}$ due to a single monopole at $\mathbf{x}''$ is given by

$$b(\mathbf{x}) = |\mathbf{w}^{\dagger}(\mathbf{x})\mathbf{C}(\mathbf{x}'')\langle a(\mathbf{x}'')\rangle|^2 \tag{7}$$

For a unit source amplitude (i.e., $|\langle a(\mathbf{x}'')\rangle|^2 = 1$), Eq. (7) is known in the literature [8] as the point-spread function of the array and is defined as

$$\mathrm{psf}(\mathbf{x}, \mathbf{x}'') = |\mathbf{w}^{\dagger}(\mathbf{x})\mathbf{C}(\mathbf{x}'')|^2 \tag{8}$$

Fixing $\mathbf{x}''$ and varying $\mathbf{x}$ through a scanning grid, the beamforming map that a single source at $\mathbf{x}''$ will produce can be obtained. Figure 1 shows the psf at 5, 10, and 25 kHz for the 63-element phased array developed at the Virginia Polytechnic Institute and State University (VT). Note that the same result is obtained by synthesizing the signals at the microphones for a monopole source of amplitude 1 and beamforming over the desired grid.

For the purpose of developing the LORE technique, the following definition of the complex point-spread function (cpsf) of the array is introduced:

$$\mathrm{cpsf}(\mathbf{x}, \mathbf{x}'') = \mathbf{w}^{\dagger}(\mathbf{x})\mathbf{C}(\mathbf{x}'') \tag{9}$$

For a single source at $\mathbf{x}''$, the beamforming output at $\mathbf{x}$ can be written as

$$b(\mathbf{x}) = |\mathrm{cpsf}(\mathbf{x}, \mathbf{x}'')\langle a(\mathbf{x}'')\rangle|^2 \tag{10}$$

As will be shown later, this new definition of a complex point-spread function is essential for an accurate modeling in the presence of multiple coherent noise sources. In the case of multiple monopole sources, the source distribution $s(\mathbf{x}')$ can be expressed as

$$\langle s(\mathbf{x}')\rangle = \sum_{m=1}^{M} \langle a(\mathbf{x}''_m)\rangle \delta(\mathbf{x}' - \mathbf{x}''_m) \tag{11}$$

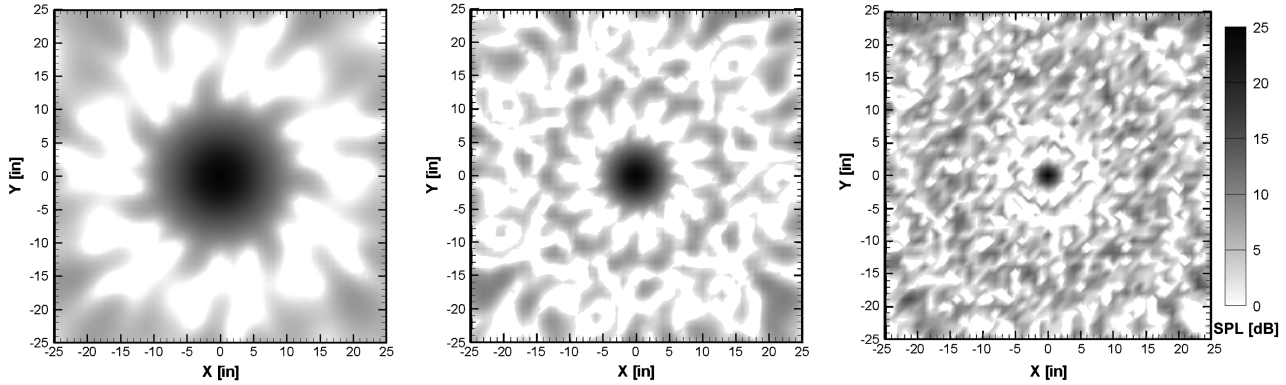

Fig. 1 Point-spread function for VT 63-element phased array at a) 5, b) 10, and c) 25 kHz.

where $\langle a(\mathbf{x}''_m)\rangle$ is the time-averaged amplitude of the source at $\mathbf{x}''_m$, and M is the number of sources.

Replacing this expression in Eq. (5), leads to

$$b(\mathbf{x}) = \left|\mathbf{w}^\dagger(\mathbf{x})\int \mathbf{C}(\mathbf{x}')\left[\sum_{m=1}^{M}\langle a(\mathbf{x}''_m)\rangle\delta(\mathbf{x}'-\mathbf{x}''_m)\right]\mathrm{d}\mathbf{x}'\right|^2$$
$$= \left|\sum_{m=1}^{M}\mathbf{w}^\dagger(\mathbf{x})\mathbf{C}(\mathbf{x}''_m)\langle a(\mathbf{x}''_m)\rangle\right|^2 \tag{12}$$

Using the definition of the cpsf, the beamformed output power at $\mathbf{x}$ is then given by

$$b(\mathbf{x}) = \left|\sum_{m=1}^{M}\mathrm{cpsf}(\mathbf{x},\mathbf{x}''_m)\langle a(\mathbf{x}''_m)\rangle\right|^2 \tag{13}$$

This expression is the basis for the technique proposed in this work. As can be seen, the relationship between the beamformed output power and the sources' amplitudes is, in general, given by a nonlinear equation. To analyze how the correlation between sources enters into the problem, this equation can be further expanded as

$$b(\mathbf{x}) = \left[\sum_{m=1}^{M}\mathrm{cpsf}(\mathbf{x},\mathbf{x}''_m)\langle a(\mathbf{x}''_m)\rangle\right]^*\sum_{m=1}^{M}\mathrm{cpsf}(\mathbf{x},\mathbf{x}''_m)\langle a(\mathbf{x}''_m)\rangle \tag{14}$$

Grouping terms that do not include cross terms in $a(\mathbf{x}'')$, Eq. (14) can be written as

$$b(\mathbf{x}) = \sum_{m=1}^{M}|\mathrm{cpsf}(\mathbf{x},\mathbf{x}''_m)|^2|\langle a(\mathbf{x}''_m)\rangle|^2$$
$$+\sum_{m=1}^{M}\sum_{\substack{s=1\\ s\neq m}}^{M}[\mathrm{cpsf}(\mathbf{x},\mathbf{x}''_m)\langle a(\mathbf{x}''_m)\rangle]^*\mathrm{cpsf}(\mathbf{x},\mathbf{x}''_s)\langle a(\mathbf{x}''_s)\rangle \tag{15}$$

As can be seen, the nonlinearity in the beamforming expression gives rise to the cross terms $\langle a(\mathbf{x}''_m)\rangle^*\langle a(\mathbf{x}''_s)\rangle$. If the sources are uncorrelated, the expected value of the cross terms is zero. If the sources are correlated, the relative phase between them is given by the difference in phase of the time-averaged source amplitudes.

In this work, it will be assumed that there is some knowledge about the problem that allows us to determine a priori if the sources are coherent or not. In this way, if the sources are assumed to be incoherent, the cross terms are zero and a linear problem can be solved. Another interesting approach that could be further studied is to include the coherence between grid points in the last term of Eq. (15), as obtained from cross-beamforming [9]. In such a case, partially correlated sources could also be accounted for in this technique.

Before introducing the proposed solution approach, it is useful to define the complex beamformed pressure as

$$y(\mathbf{x}) = \sum_{m=1}^{M}\mathrm{cpsf}(\mathbf{x},\mathbf{x}''_m)\langle a(\mathbf{x}''_m)\rangle \tag{16}$$

The advantage of this form is that the equation is linear. Then the complex beamformed pressure is related to the actual beamforming output $b(\mathbf{x})$ as

$$b(\mathbf{x}) = |y(\mathbf{x})|^2 = y(\mathbf{x})^* y(\mathbf{x}) \tag{17}$$

With the previous definition, the complex beamformed pressure over a set of N points due to M sources in the scanning field can be expressed in matrix form as

$$\begin{Bmatrix} y(\mathbf{x}_1)\\ y(\mathbf{x}_2)\\ \vdots\\ y(\mathbf{x}_N)\end{Bmatrix} = \begin{bmatrix} \mathrm{cspf}(\mathbf{x}_1,\mathbf{x}''_1) & \mathrm{cspf}(\mathbf{x}_1,\mathbf{x}''_2) & \dots & \mathrm{cspf}((\mathbf{x}_1,\mathbf{x}''_M)\\ \mathrm{cspf}(\mathbf{x}_2,\mathbf{x}''_1) & \mathrm{cspf}(\mathbf{x}_2,\mathbf{x}''_2) & \cdots & \mathrm{cspf}(\mathbf{x}_2,\mathbf{x}''_M)\\ \vdots & \vdots & \ddots & \vdots\\ \mathrm{cspf}(\mathbf{x}_N,\mathbf{x}''_1) & \mathrm{cspf}(\mathbf{x}_N,\mathbf{x}''_2) & \cdots & \mathrm{cspf}(\mathbf{x}_N,\mathbf{x}''_M)\end{bmatrix}$$
$$\times\begin{Bmatrix}\langle a(\mathbf{x}''_1)\rangle\\ \langle a(\mathbf{x}''_2)\rangle\\ \vdots\\ \langle a(\mathbf{x}''_M)\rangle\end{Bmatrix} \tag{18}$$

Because the number of sources in the scanning field is generally unknown, the number of sources must be assumed to be equal to the number of scanning points (i.e., $M = N$). This will render a square matrix in the previous equation. At this point, it should be clear that the similarity to image processing is in the sense that the beamforming maps (images) for single sources are being superimposed in complex form to obtain the actual beamforming map.

It is important to note that if the sources are correlated, the source amplitudes $\langle a(\mathbf{x}''_m)\rangle$ for $m = 1,\dots,N$ must be assumed to be complex in Eq. (18) to account for relative phase information. However, note that the beamforming output (power) $b(\mathbf{x})$, and hence $y(\mathbf{x})$ obtained from it as $y(\mathbf{x}) = \sqrt{b(\mathbf{x})}$, lack phase information. Thus, it is not possible to solve Eq. (18) to find the sources strength if $y(\mathbf{x})$ is obtained from the beamforming output $b(\mathbf{x})$. An alternative solution approach that is capable of determining phase information is proposed next.

III. Solution Approach

As seen before, the modeling of the beamforming output for coherent sources renders a system of nonlinear equations in terms of the time average of the sources' amplitudes [i.e., $\langle a(\mathbf{x}''_m)\rangle$ for $m = 1,\dots,N$]. Because the size of the system is given by the number of scanning grid points N, the problem has a very large number of unknowns. This problem could be solved using Newton–Raphson method. However, a good initial guess would be required for every

point in the grid and computing the Jacobian might be computationally expensive for big systems. Another approach would be to use a nonlinear optimization technique for all of the grid points. This approach would also have similar limitations in terms of initial guess and computational time.

To overcome these issues and solve the nonlinear problem for coherent sources, a new two-step approach is proposed in this work. These steps are as follows:

1) Solve an approximated linear problem (i.e., a relaxed version). Solving this approximated model will reduce the number of sources in the grid (i.e., only potential noise sources will have source strength different from zero). The approach taken here finds the sources' amplitudes for a linearized model (i.e., assuming incoherence) solving a least-squares problem with nonnegativity constraints.

2) Solve the nonlinear problem using an optimization procedure. This is accomplished by optimizing only the nonzero values obtained in step 1. In this work, the multidimensional optimization problem was implemented using the downhill simplex method. Because a reduced number of points are being optimized, the computational time is significantly reduced when compared with optimizing the set of all grid points. In the case of incoherent sources, the system to optimize is linear and this step can be omitted or used to improve computational speed, as will be explained later.

The proposed solution approach is illustrated in Fig. 2. As can be seen, the initial point of the procedure is the beamforming output for every single point in the grid. Solving the approximated problem in step 1 would render a much smaller number of potential noise sources (i.e., a reduced set of nonzero grid points). The application of the optimization procedure described in step 2 to the nonzero values from step 1 would render only the actual noise sources' levels and positions (i.e., zeroing out all the potential sources that are not actual sources). As can be observed, the results from LORE are much cleaner and thus easier to interpret than the beamforming output (i.e., side lobes are not present and the actual levels can be recovered).

Note that in this work, the time-averaged source amplitudes $\langle a(\mathbf{x}''_m)\rangle$ are plotted in decibel scale as obtained from

$$A_m \text{ dB} = 10 \times \log_{10}\left(\frac{\langle a(\mathbf{x}''_m)\rangle^* \langle a(\mathbf{x}''_m)\rangle}{2}\right) \tag{19}$$

A. Solve an Approximated Linear Problem

As mentioned before, the key idea in step 1 of the LORE technique is to discard as many grid points as possible for which the amplitude is most likely to be zero. Thus, only potential noise sources are kept for the optimization procedure in step 2. The approach is to find an approximated linear problem and solve it using a least-squares approach. To this end, the cross terms $\langle a(\mathbf{x}''_m)\rangle\langle a(\mathbf{x}''_s)\rangle$ in Eq. (15) are neglected (i.e., the sources are assumed to be incoherent). The following linear equation is then obtained:

$$b'(\mathbf{x}) = \sum_{m=1}^{M} |\text{cpsf}(\mathbf{x}, \mathbf{x}''_m)|^2 \langle |a(\mathbf{x}''_m)|\rangle^2 \tag{20}$$

Note that for incoherent sources, $b'(\mathbf{x})$ is the actual beamforming output and the solution to this system is already the actual solution. Equation (20) is also equivalent to the linear system solved using DAMAS [1]. However, for incoherent sources, $b'(\mathbf{x})$ is only an approximation to the actual beamforming output $b(\mathbf{x})$, and thus the solution to the linearized system is not the correct answer.

In matrix form, Eq. (20) can be written as

$$\begin{Bmatrix} b'(\mathbf{x}_1) \\ b'(\mathbf{x}_2) \\ \vdots \\ b'(\mathbf{x}_N) \end{Bmatrix} = \begin{bmatrix} |\text{cspf}(\mathbf{x}_1,\mathbf{x}''_1)|^2 & |\text{cspf}(\mathbf{x}_1,\mathbf{x}''_2)|^2 & \dots & |\text{cspf}((\mathbf{x}_1,\mathbf{x}''_N)|^2 \\ |\text{cspf}(\mathbf{x}_2,\mathbf{x}''_1)|^2 & |\text{cspf}(\mathbf{x}_2,\mathbf{x}''_2)|^2 & \cdots & |\text{cspf}(\mathbf{x}_2,\mathbf{x}''_N)|^2 \\ \vdots & \vdots & \ddots & \vdots \\ |\text{cspf}(\mathbf{x}_N,\mathbf{x}''_1)|^2 & |\text{cspf}(\mathbf{x}_N,\mathbf{x}''_2)|^2 & \cdots & |\text{cspf}(\mathbf{x}_N,\mathbf{x}''_N)|^2 \end{bmatrix} \times \begin{Bmatrix} |\langle a(\mathbf{x}''_1)\rangle|^2 \\ |\langle a(\mathbf{x}''_2)\rangle|^2 \\ \vdots \\ |\langle a(\mathbf{x}''_N)\rangle|^2 \end{Bmatrix} = [\hat{\mathbf{E}}] \begin{Bmatrix} |\langle a(\mathbf{x}''_1)\rangle|^2 \\ |\langle a(\mathbf{x}''_2)\rangle|^2 \\ \vdots \\ |\langle a(\mathbf{x}''_N)\rangle|^2 \end{Bmatrix} \tag{21}$$

Equation (21) is a linear system of equations that needs to be solved to obtain the sources' power [i.e., $|\langle a(\mathbf{x}''_m)\rangle|^2$]: thus, a solution that is constrained to be positive. This constraint is physically correct because there cannot be an acoustic source with negative power. In the LORE approach, this problem is solved using the nonnegative least-squares (NNLS) algorithm developed by Lawson and Hanson [10], posed as

$$\min_{\langle |\mathbf{a}(\mathbf{x}''_m)|\rangle} \frac{1}{2} \left\| \hat{\mathbf{E}} |\langle \mathbf{a}(\mathbf{x}''_m)\rangle|^2 - \mathbf{b} \right\|_2^2 \tag{22}$$

with the constraint $|\langle a(\mathbf{x}''_m)\rangle|^2 \geq 0$, where the values for $\mathbf{b}'$ were replaced with those from the actual beamforming output $\mathbf{b}$.

It is now important to prove that using this approximation for coherent sources, an appropriate solution is obtained to be used as a starting point for the optimization in step 2. The key issue is to have confidence that actual noise sources are not assigned a zero value (i.e., discarding grid points related to actual noise sources). To this end, the solution from the original model shown in Eq. (15) will be compared with the approximated one in Eq. (20).

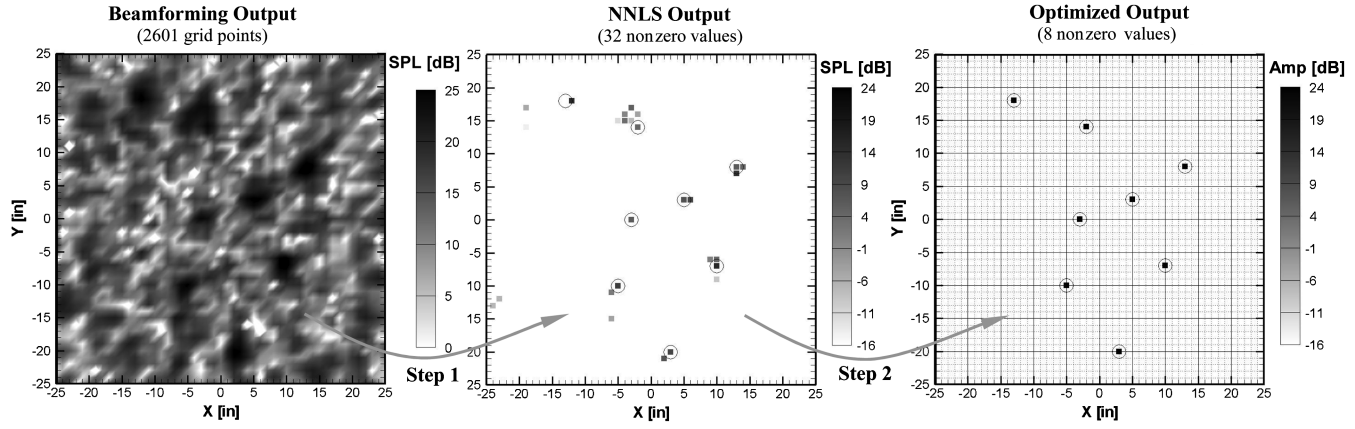

Fig. 2 Schematic of the results obtained in the two-step LORE technique (actual simulation and coherent sources).

Using the triangle inequality property of the norms, the following relation can be expressed:

$$\left|\sum_m \text{cpsf}(\mathbf{x}, \mathbf{x}''_m)\langle a(\mathbf{x}''_m)\rangle\right|^2 \leq \sum_m |\text{cpsf}(\mathbf{x}, \mathbf{x}''_m)|^2 |\langle a(\mathbf{x}''_m)\rangle|^2 \quad (23)$$

Hence,

$$b(\mathbf{x}) \leq b'(\mathbf{x}) \quad (24)$$

Note that the equality holds only in the case of a single source or incoherent sources. Because the values for $b'(\mathbf{x})$ in Eq. (22) are replaced with the actual beamforming output $b(\mathbf{x})$, the NNLS procedure will actually find the minimum $|\langle a(\mathbf{x}''_m)\rangle|^2$ for $m = 1, \ldots, N$ that satisfies

$$b(\mathbf{x}_n) = \sum_{m=1}^{M} |\text{cpsf}(\mathbf{x}_n, \mathbf{x}''_m)|^2 |\langle a(\mathbf{x}''_m)\rangle|^2, \qquad n = 1, \ldots, N \quad (25)$$

Then the solution from the least-squares problem will be such that the sources' power is always underpredicted for coherent sources [i.e., smaller than the actual solution to satisfy the inequality in Eq. (24)].

The fact that actual noise sources are not discarded is related to the procedure that NNLS uses to add potential variables to the set of nonzero values (i.e., satisfying the Kuhn–Tucker conditions [11]). As a result, the number of grid points assigned a nonzero value should be greater than or equal to the actual number of sources. As will be shown later for some particular coherent source distributions, some issues are present when side lobes are higher than lobes for actual sources. As a consequence, the actual sources' locations might not be correctly found (i.e., the sources shifted from their actual positions).

B. Solve the Nonlinear Problem Using an Optimization Procedure

As mentioned before, this step is only required for coherent sources, because the output of step 1 already renders the correct answer in the case of incoherent sources. However, it was found that the results' accuracy and processing speed can be improved if the NNLS is applied with a lower error threshold and optimization is used on the linear system to find the exact answer. The following description of the method shows the approach for the case of coherent sources, but a similar approach can be developed for optimizing incoherent sources in the linear system.

Note that at this point, two different options are available to obtain the solution for coherent sources. One of them would be to optimize all the points in the grid using the results from step 1 as the initial guess. This would guarantee that none of the actual sources is wrongfully assigned with zero amplitude. However, as mentioned before, this might require extensive computations that would make the approach impractical. The other option is to perform an optimization only over the NZ nonzero values of $\langle a(\mathbf{x}''_m)\rangle$ obtained from step 1. The latter approach was implemented in this work.

To this end, a modification of the Nelder and Mead simplex method [11–13] was implemented. Such modifications define the stopping criteria and the subspace in which the solution is being optimized. With the results from the previous step, the system to optimize is then given by N nonlinear equations with NZ unknowns of the form shown in Eq. (13). Thus,

$$b(\mathbf{x}_n) = \left|\sum_{m=1}^{\text{NZ}} \text{cpsf}(\mathbf{x}_n, \mathbf{x}''_m)\langle a(\mathbf{x}''_m)\rangle\right|^2, \qquad n = 1, \ldots, N \quad (26)$$

As mentioned before, there are no restrictions in this equation. Thus, the sources' incoherence assumption is not present. To improve computational time by implementing a matrix multiplication, the expression with the complex beamformed pressures Y is used instead of the beamforming output power b. Thus, a tall, skinny system of the following form is obtained:

$$\begin{Bmatrix} y(\mathbf{x}_1) \\ y(\mathbf{x}_2) \\ \vdots \\ y(\mathbf{x}_N) \end{Bmatrix} = \begin{bmatrix} \text{cspf}(\mathbf{x}_1, \mathbf{x}''_1) & \text{cspf}(\mathbf{x}_1, \mathbf{x}''_2) & \ldots & \text{cspf}((\mathbf{x}_1, \mathbf{x}''_{\text{NZ}}) \\ \text{cspf}(\mathbf{x}_2, \mathbf{x}''_1) & \text{cspf}(\mathbf{x}_2, \mathbf{x}''_2) & \cdots & \text{cspf}(\mathbf{x}_2, \mathbf{x}''_{\text{NZ}}) \\ \vdots & \vdots & \ddots & \vdots \\ \text{cspf}(\mathbf{x}_N, \mathbf{x}''_1) & \text{cspf}(\mathbf{x}_N, \mathbf{x}''_2) & \cdots & \text{cspf}(\mathbf{x}_N, \mathbf{x}''_{\text{NZ}}) \end{bmatrix} \times \begin{Bmatrix} \langle a(\mathbf{x}''_1)\rangle \\ \langle a(\mathbf{x}''_2)\rangle \\ \vdots \\ \langle a(\mathbf{x}''_{\text{NZ}})\rangle \end{Bmatrix} \quad (27)$$

where, in general, $N \gg \text{NZ}$.

Note that if phase information could be obtained for the complex beamformed pressure y from the beamforming output power b, solving a nonlinear problem could be avoided [i.e., solving the complex system of linear equations shown in Eq. (27)].

Because it was assumed that coherent sources are present, the optimization involves a system of NZ equations of the form

$$\xi_n = b(\mathbf{x}_n) - \left|\sum_{m=1}^{\text{NZ}} \text{cpsf}(\mathbf{x}_n, \mathbf{x}''_m)\langle a(\mathbf{x}''_m)\rangle\right|^2 \quad (28)$$

where $\langle a(\mathbf{x}''_m)\rangle$ are complex numbers, thus resulting in $2 \times \text{NZ}$ values to be optimized [i.e., corresponding to the real and complex components of $\langle a(\mathbf{x}''_m)\rangle$]. The initial guesses are the real nonzero values obtained from the NNLS solution. The function to minimize in the optimization is the norm of the total relative error given by

$$f(\mathbf{b}, \mathbf{a}) = \frac{\left(\sum_{n=1}^{N} \xi_n^2\right)^{1/2}}{\max_i |b_i|} \quad (29)$$

To further reduce the number of parameters to optimize in step 2, the theoretical array SNR can be used. Thus, values of $\langle a(\mathbf{x}''_m)\rangle$ that are smaller than the theoretical array SNR (or times a factor) from the maximum value can be discarded after step 1 to reduce computational time. However, in some complex cases, this has proven to discard actual noise sources, especially in 3-D cases; hence, it is not recommended.

The reader should at this point realize that the authors do not think the NNLS or the optimization techniques used in this work are the best solutions to the problem in terms of accuracy and computational speed. However, given the complexity of the posted problem, a practical-solution approach should be proposed. A clear improvement could be to replace the current optimization technique with a more sophisticated approach. Another improvement would be to investigate a different approach for step 1 such as to not restrict the solution only to the points found with the NNLS. As mentioned before, one such approach would be to optimize the entire grid using the NNLS solution as the initial guess, but this approach might not be practical in terms of the time required to obtain a solution. In some other cases, it might be possible to restrict the solution to a known subset of points. For instance, nonzero values are assigned arbitrarily only to the grid points of the trailing edge, and the optimization is performed only on such points. A similar idea is proposed in DAMAS-C [5], referred to as problem reduction by zoning. Of course, this implies assuming something about the problem beforehand that would result in a restriction of the solution space and might lead to accuracy loss.

IV. Estimation of Results Accuracy

To evaluate the quality of the results from LORE, it is proposed to compare a reconstruction of the beamforming map to the actual one. The reconstruction of the results consists of using the amplitudes obtained with LORE and feeding them into the model of Eq. (15) to obtain the reconstructed beamforming map. In this way, the accuracy of the results can be determined by comparing the actual

and reconstructed beamforming maps. Even when visual comparison of the maps is very helpful, an automated procedure that gives a measure of how much these images are alike is preferred (i.e., a single numerical value giving an estimate of the accuracy of the LORE results).

In image processing, a common practice to determine if two images are similar is to use the correlation coefficient [14–16]. If both maps are identical, the correlation will be equal to 1. If there are differences, the correlation will be lower. This correlation metric is a particular case of feature detection [17,18] in which both images have the same size (i.e., same number of grid points).

Because the beamforming output in linear scale has a large range that does not allow recognizing differences in the maps, the comparison of the actual and reconstructed beamforming maps is performed in decibel scale (i.e., as one would visually compare the maps to determine if they are similar). The correlation coefficient relating the actual and reconstructed beamforming maps is then given by

$$C = \frac{\sum_{i=1}^{N} 10\log_{10}(b(\mathbf{x}_i))10\log_{10}(b_R(\mathbf{x}_i))}{\sqrt{\sum_{i=1}^{N} 10\log_{10}(b(\mathbf{x}_i))\sum_{i=1}^{N} 10\log_{10}(b_R(\mathbf{x}_i))}} \tag{30}$$

where $b(\mathbf{x}_i)$ and $b_R(\mathbf{x}_i)$ are, respectively, the actual and reconstructed beamforming output at the point $\mathbf{x}_i$.

The results from LORE are considered to be satisfactory if the correlation coefficient is greater than 0.9. The reconstructed maps will be shown in addition to the correlation coefficient for the cases in which it is considered helpful in the understanding of the results and limitations from LORE. Note that in terms of the energy, a correlation coefficient of 1 is equivalent to recovering 100% of the power on the map. However, recovering 100% of the power does not imply that the maps for the deconvoluted sources represent the same map/energy distribution as the actual sources (i.e., correlation could be less than 1). For the results presented in this work, the total power in the maps (i.e., adding the output for all grid points) was also computed and compared with the reconstruction. It was found that for correlation coefficients higher than 0.9, the recovered power for the entire map is within 0.5 dB.

V. Numerical Simulations

The numerical simulations presented in this section are organized by increasing level of difficulty, thus starting from the simplest cases and adding complexity in each step. For every case, the beamforming output was obtained by generating the time-domain signals for each microphone of the array. The time-domain signals were then taken to the frequency domain and the corresponding cross-spectral matrix (CSM) was calculated. For incoherent sources, 50 averages with a random phase on each source were used to compute the CSMs. Conventional beamforming was then applied to a grid of 25 by 25 in. in a plane 36 in. parallel to the array. The grid resolution used was 1 in., thus resulting in 2601 scanning points. As shown before, this also determines the size of the system to solve in the LORE technique. Unless otherwise stated, the amplitude of the sources was set to 23.9 dB, as obtained from Eq. (19). For ease of visualization, a cutoff was applied to the LORE results. The actual position of the sources is denoted using a black circle around the corresponding grid point. Dashed circles are used to denote artificial sources (i.e., grid points with amplitude not equal to zero and not associated with actual noise sources).

The computational time indicated in the following examples is shown only as a reference and was obtained using a dual-core (1.83 GHz) laptop computer with no parallel processing (i.e., a single core was used). No direct comparison was established with other techniques for the same cases; however, keep in mind that the time reported for DAMAS in the literature for a single source is on the order of minutes [1], and for some complex cases it was reported to be on the order of hours or days [3].

A. Single Source

The first case analyzed is a single monopole source in the center of the scanning grid. As can be seen in Fig. 3a, the beamforming map shows a clear noise source at the center of the scanning grid, and the worst side lobe appears to be 10 dB below the main lobe. Applying the LORE technique, the results shown in Fig. 3b are obtained. As can be seen, the only nonzero value is at the grid point at which the actual noise source is present. Its amplitude is also successfully recovered. The correlation for this case is equal to 1, as expected. The time needed for this computation is less than 30 s.

The second case to be analyzed is a single source for which the actual position is not in a grid point (i.e., between grid points at 0.5, 0.5, and 36 in.). The results are shown in Fig. 4. Note that there are no big changes in the beamforming map when compared with the previous case. However, the maximum level is slightly lower (about 1 dB).

Figure 4b shows a detail of the LORE results in the region in which the source is located. As can be seen, the solution renders four sources around the actual noise source position. In this case, the actual source amplitude is obtained by adding the values at those points. As indicated in the figure, the recovered level (24.15 dB) is slightly higher than the actual level (23.9 dB). The correlation factor for this case is 0.965; thus, the results are expected to have a small error. Evidently, this error would be reduced if a finer grid were to be used. The computational time for this case was only 21 s.

The case of a single monopole source is trivial, and the results are correctly rendered for any frequency. However, the real challenge is obtaining results in the presence of multiple and/or coherent sources, as will be presented in following sections.

B. Multiple Scattered Incoherent Sources

This section presents results for the case of multiple incoherent sources. As seen in the formulation, if the sources are incoherent, the expected value of the cross terms is zero [i.e., $\langle a(\mathbf{x}''_m)\rangle\langle a(\mathbf{x}''_s)\rangle$]. However, in real life, the expected value is replaced by a finite number of averages that are not zero. This is a downfall that all deconvolution methods based on the theoretical psf suffer. As a

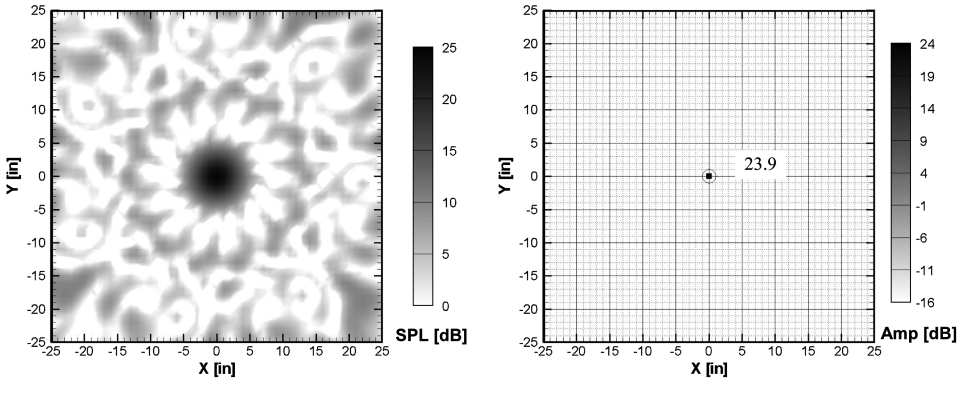

Fig. 3 Single source at a grid point (10 kHz): a) beamforming and b) LORE results.

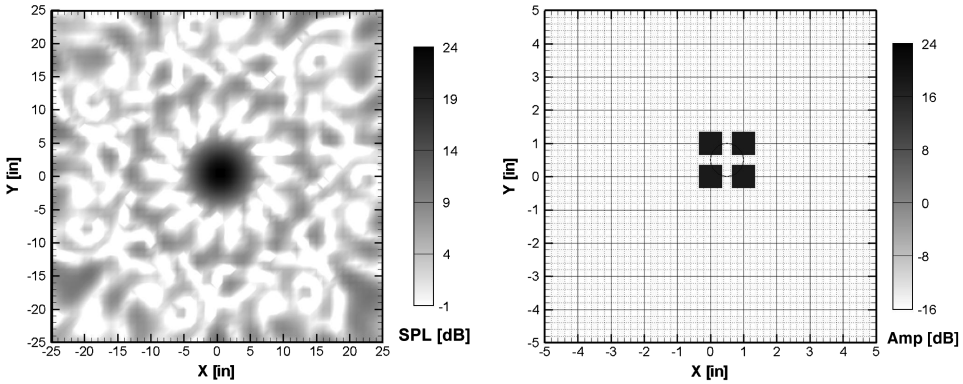

a) b)

Fig. 4 Single source (10 kHz) between grid points (i.e., $X = 0.5$ and $Y = 0.5$): a) beamforming and b) detail of LORE results.

result, the accuracy of the results depends on the number of averages used in the simulation or acquired during testing.

Figure 5 shows the beamforming map at 15 kHz for eight sources with the same level (23.9 dB) using 20, 50, and 100 averages, respectively. As can be seen, the number of averages clearly affects the maps in terms of levels and side-lobe structure. Note also that the array SNR is significantly reduced when multiple coherent sources are present. As a result, the position of all of the actual noise sources is not clear, due to the presence of many side lobes with relatively high levels (i.e., many were around 3–6 dB below the maximum level of the map when the SNR for a single source was about 12 dB).

The postprocessing results for these three cases are shown in Fig. 6. The results show that accuracy is improved and the number of artificial sources is reduced when the number of averages is increased.

As mentioned before, an interesting insight can be obtained by visually comparing the reconstructed and actual beamforming maps. Thus, analyzing how similar the maps are, some conclusions could be stated about the accuracy of the postprocessing solution and the reason for eventual discrepancies. This is especially true for complex source distributions and at low frequencies. In this sense, Fig. 7 shows the comparison between the actual and reconstructed beamforming maps for the case of 50 averages. As can be seen, there are only minor differences between the maps. This was expected because the number and levels of artificial sources were not significant and the correlation factor was equal to 0.969.

C. Line of Sources

This section presents results obtained for a linear distribution of incoherent sources using 50 averages in the simulation. Such distribution consists of seven sources 1 in. apart, each with an amplitude of 23.9 dB. Figure 8 shows the beamforming maps for the numerical simulations at 25, 15, and 10 kHz, respectively. Note that

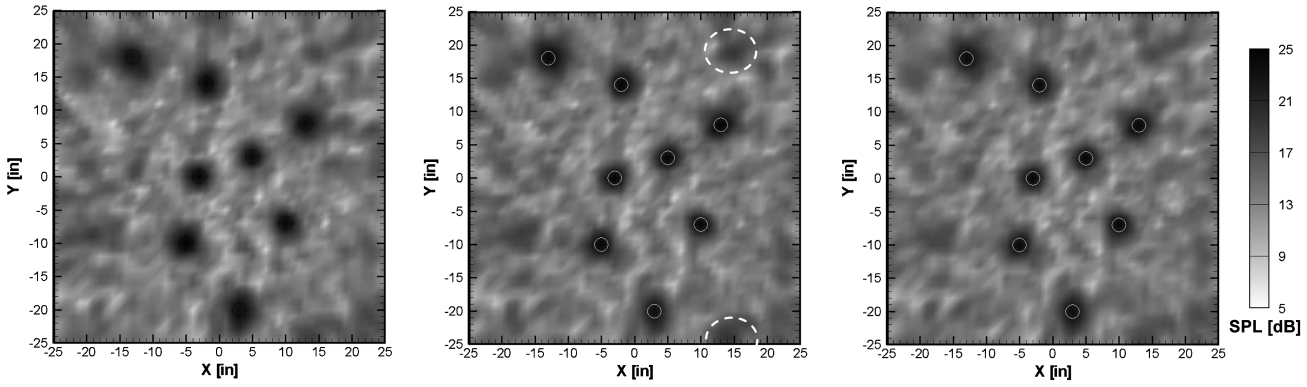

a) b) c)

Fig. 5 Simulation of eight scattered incoherent sources at 15 kHz using a) 20, b) 50, and c) 100 averages.

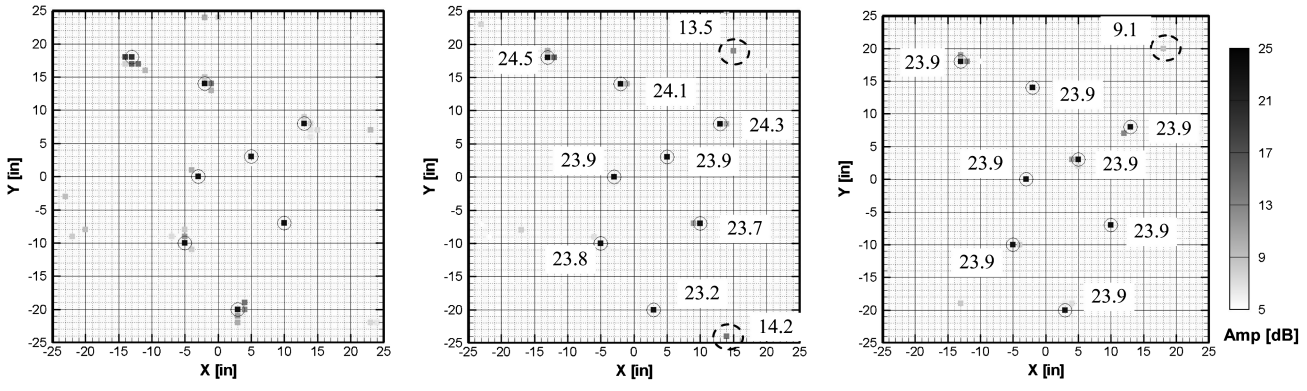

a) b) c)

Fig. 6 LORE results for eight scattered incoherent sources at 15 kHz using a) 20, b) 50, and c) 100 averages.

in all cases, the actual number of sources and levels cannot be identified from the maps.

The LORE results for these cases are shown in Fig. 9. In this case, as in the following examples, the black circles mark the actual position of the noise sources. As can be seen, the position and level of each individual source were successfully determined with an error less than 1.7 dB on their individual levels. Considering the line of sources as a single source, the error in total levels was about 0.3 dB at 25 kHz, 0.15 dB at 15 kHz, and less than 0.05 dB at 10 kHz. The correlation coefficient was at least 0.966, improving at lower frequencies. The processing time ranged from 27 to 34 s.

The same case for a frequency of 5 kHz is presented in Fig. 10. Even when the maps resemble that of a single source, LORE results still show some kind of linear spreading of the source. Given the size of the array, the lack of resolution in the maps (and hence in the LORE results) were expected at this frequency. This is related to the fact that at lower frequencies, more grid points are within the main lobe. Hence, for a given error threshold, the solution space is larger. The actual total level of the sources distribution is successfully recovered (i.e., 32.3 dB compared with the actual 32.4). The correlation coefficient in this case was 0.997, indicating a very good result. The computational time in this case was about 31 s.

The effect of increasing the grid size was not studied in this case, but it should also improve the results at low frequencies. Thus, the side-lobe patterns that would appear in a bigger beamforming map may help in rendering more accurate results. This is related to the fact that the levels and positions of the side lobes for a single source are different from those for a source distribution such as that used in this case.

D. Coherent Sources

As mentioned in the theoretical development of the LORE technique, even though phase information is not available in the beamforming output, it can be assumed that the sources are coherent and obtain the correct results in terms of amplitude and relative phase.

As shown in Fig. 11, the beamforming maps are significantly different for coherent and incoherent sources as well as for coherent sources with different relative phases. In all cases, the amplitude of each source was set to 23.9 dB. Similar results for coherent sources can be seen in the work by Horne et al. [9], in which the effect of correlation on the beamforming output was studied. This difference in the maps also suggests that the reconstruction from LORE could be used to determine if the coherence assumption was correct in the first place for solving a given problem.

If the dipole case were to be solved assuming that the sources are incoherent, the results shown in Fig. 12a would be rendered. In this particular case, the levels of all nonzero grid points around the actual source positions add up to 23.4 dB. However, in a different case (i.e., number of sources, distribution, frequency, or relative phase), the difference to the actual values could be more significant. Note that the correlation coefficient in this case was only 0.85, indicating that the incoherence assumption is erroneous.

If no assumptions are made about the incoherence of the sources in the LORE processing, the results shown in Fig. 12b are obtained. In this case, the levels and positions are successfully recovered. Note that in both cases, the optimization procedure starts with the same set of 16 points from the NNLS step. The computational time is now about 24.7 s. To obtain the total levels in the case of coherent sources, all the nonzero grid points in the source region are added in complex form. The worst artificial source in this case was −51 dB (i.e., 75 dB below the level of the actual sources). For coherent sources, the LORE technique also renders the phase information. In this case, the relative phase between the major sources was found to be 180 deg. The phase information is shown in Fig. 12c. As can be seen, other sources appear with a difference phase, but keep in mind that their levels are negligible when compared with the actual levels. As expected, the correlation coefficient in this case is much closer to 1 (i.e., 0.9999995), indicating that the results are very accurate.

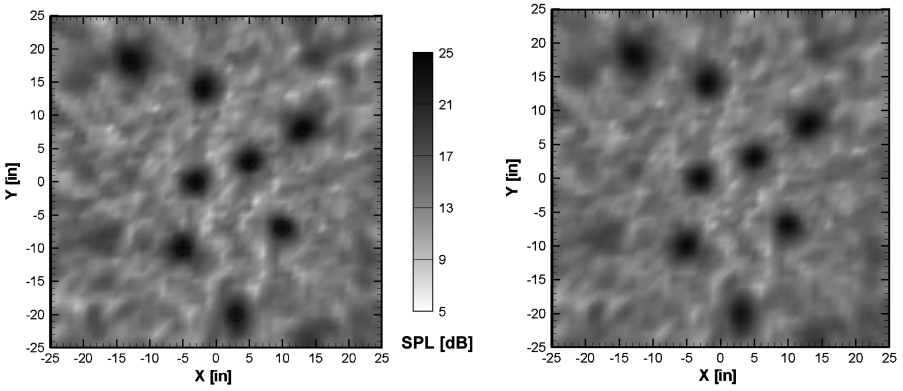

Fig. 7 Simulation of eight scattered incoherent sources at 15 kHz using 50 averages. Comparison between a) beamforming and b) reconstruction from LORE modeling.

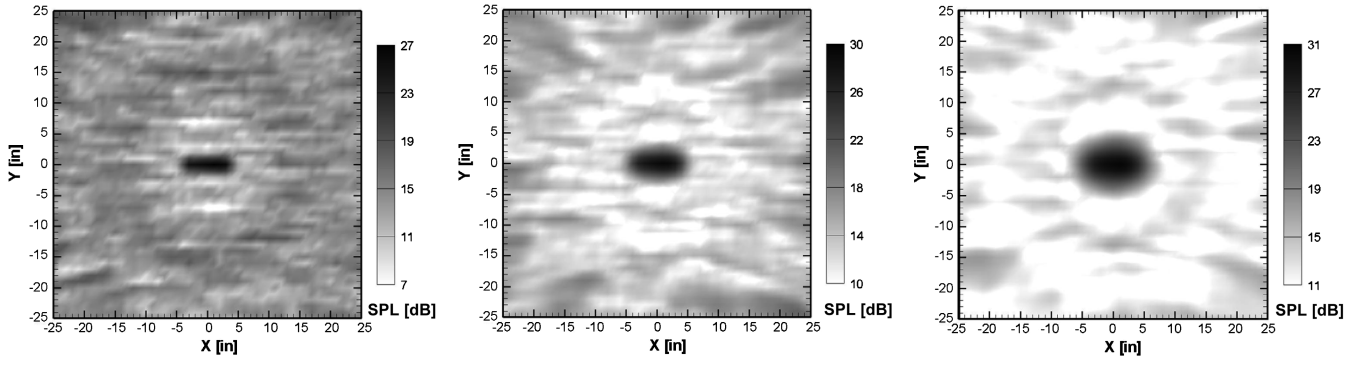

Fig. 8 Beamforming maps for a line of seven sources 1 in. apart at a) 25, b) 15, and c) 10 kHz.

It is interesting to analyze the case of multiple coherent sources. In particular, a linear distribution of coherent sources will be analyzed (i.e., similar to coherent trailing-edge noise). Figure 13a shows the beamforming map for five coherent sources 2 in. apart. The relative phase between the sources was set to −90, −45, 0, 45, and 90 deg, respectively, from left to right. The amplitude of all sources is the same and equal to 23.9 dB. As can be seen, the beamforming map looks irregular when compared with the results for a line of incoherent sources, as in Fig. 8b.

If this case is postprocessed assuming that the sources are incoherent, the LORE results presented in Fig. 13b are rendered. In this case, the results do not agree with the simulated source distribution, reflected in a low correlation coefficient of 0.638 and an overall level of the sources in the center of about 32 dB compared with the actual 37.9 dB. Note that there are also many artificial sources with relatively high levels. A similar erroneous result would be obtained using a postprocessing technique that does not account for coherent sources.

If no assumptions are made about the coherence of the sources, LORE can render the actual levels and source positions, as shown in Fig. 14a. The level of the worst artificial source in this case was −35 dB (i.e., 59 dB lower in power than a single actual source). The power of the actual noise sources adds up to 37.89 dB, instead of the actual 37.9 dB.

As shown in Fig. 14b, LORE results show that the sources have a relative phase of about 45 deg with the adjacent sources: thus, in very good agreement with the simulated sources. The accuracy of the results is also reflected in a correlation coefficient of 0.9999996.

It was found that in the presence of several scattered noise sources, the results may lose accuracy in terms of source position. This is related to the increasing number of variables to optimize and the ill-conditioning of the matrix of cpsfs. Keep in mind that the rank of the matrix of cpsfs is related to the actual number of sources, and a larger number of potential sources are usually being minimized.

VI. Experimental Results

It was shown in previous sections that LORE is able to successfully recover the positions and actual levels of the sources in the scanning field for a wide range of frequencies. This ability is related to the accuracy of the modeling proposed in this work. However, when dealing with experimental data, the signals are usually contaminated with noise. At the same time, this contaminating noise can be uncorrelated or partially correlated over the array [9]. In real life, the fact that the array is not perfect also needs to be taken into account. Thus, because phase and positioning errors of the microphones are present, the experimental point-spread function will depend on the array calibration (i.e., response for a single source). As suggested by Sijtsma [6], these factors will influence the accuracy of the results. Keep in mind that LORE relates the experimental beamforming output to the theoretical response of the array. The quality of the expected results from LORE can be assessed by analyzing the case of a single source in the anechoic chamber (i.e., comparing the experimental beamforming map with the numerical simulation of a single source in the same position). As shown before, the reconstruction from the LORE processing can also be used to determine the quality of the results.

To test the capabilities of LORE with experimental data, a series of tests were conducted. The test consisted of placing multiple speakers in the VT anechoic chamber and measuring with a 63-element equal-aperture multi-arm spiral array. The speakers used in this test are University Sound model ID60C8. Their directionality was not measured for these series of tests (i.e., they were assumed to be point sources). The speakers were driven with different signal generators to generate uncorrelated sources, and a single generator with equipment to adjust the relative phase was used to create correlated sources. The array output was not calibrated in level. The test setup is shown in Fig. 15.

Figure 16a shows the test configuration for a single speaker. In this case, as well in the following one, the speakers that are on are

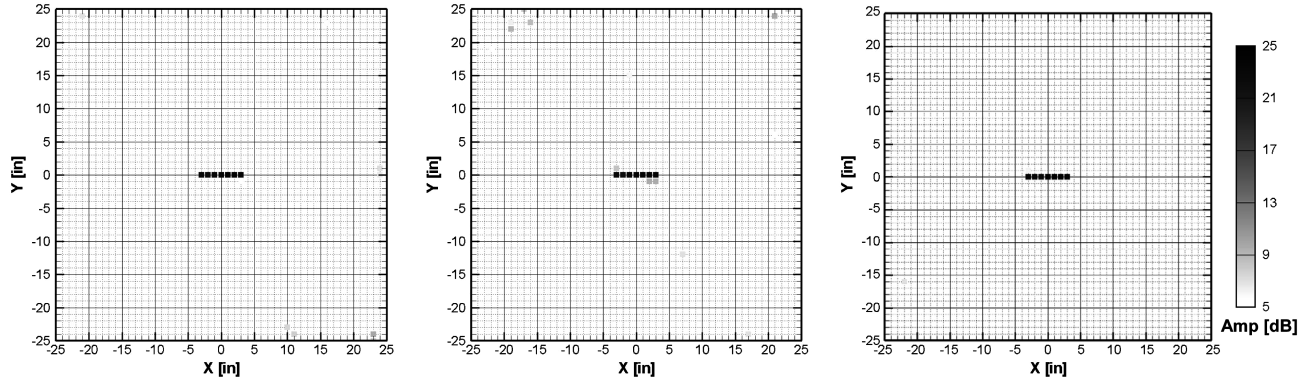

a) b) c)

Fig. 9 LORE results for a line of sources at a) 25, b) 15, and c) 10 kHz.

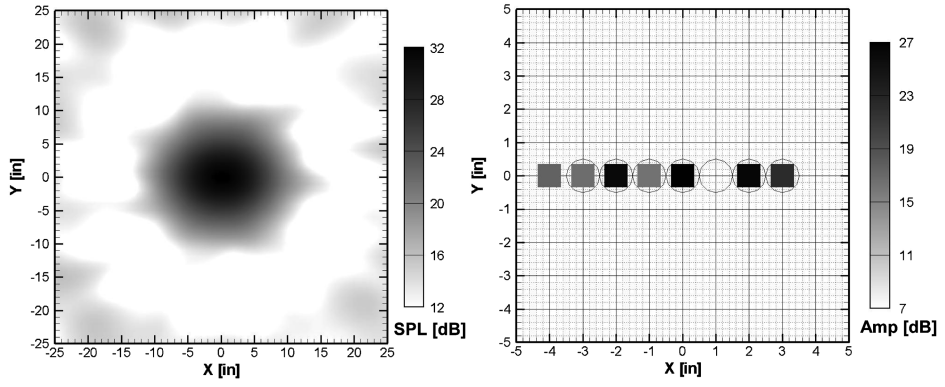

a) b)

Fig. 10 Plots of the a) beamforming map for a line of seven sources 1 in. apart at 5 kHz and b) detail of LORE results.

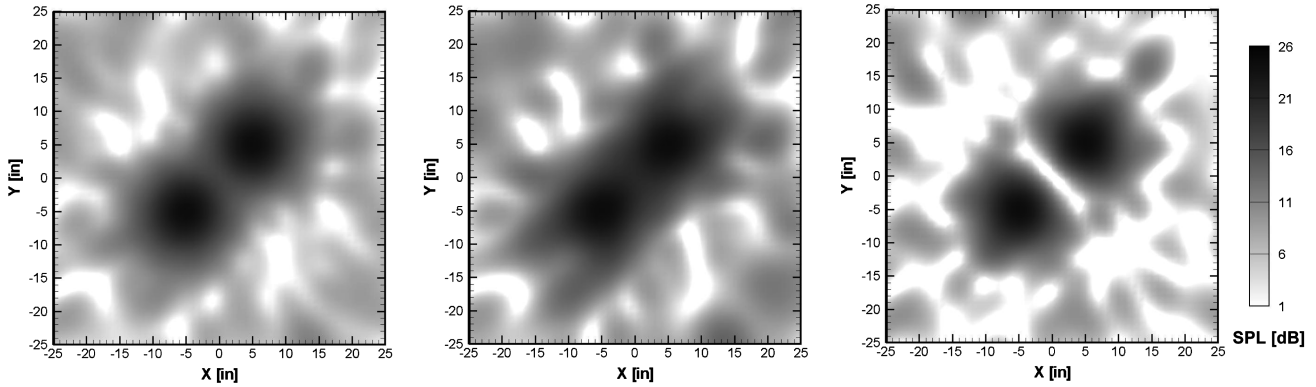

Fig. 11 Beamforming simulation for two sources at 5 kHz: a) incoherent, b) coherent with 0 deg relative phase, and c) coherent with 180 deg relative phase (i.e., dipole).

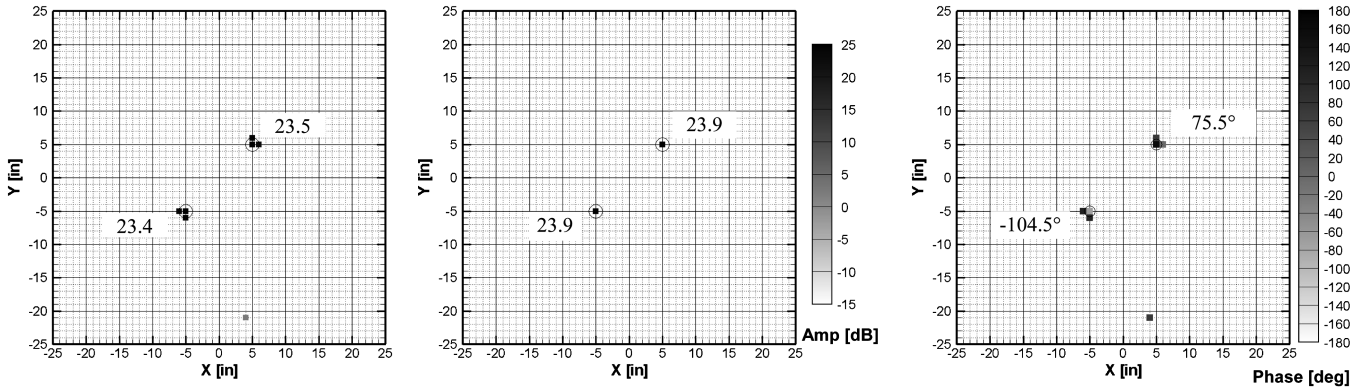

Fig. 12 LORE results for a dipole at 5 kHz assuming a) incoherence, b) coherence, and c) phase information obtained in LORE assuming coherence.

indicated with a circle and those that are off are indicated with a crossed-out circle. Figure 16b shows the beamforming map at 2.2 kHz. For ease of visualization and interpretation, the images showing the configuration of the speakers are mirrored to plot the results in the X–Y plane in the form indicated in Fig. 15.

Figure 17a shows the LORE results for a grid 20 by 20 in. with a grid resolution of 1 in. As can be seen, the method is able to recover a cluster of three sources at the center of the grid with a level of 98.9 dB. As seen in simulations, this kind of result would suggest that the source is not exactly at the center of the grid. Note also that there are artificial sources in the corners of the grid. The maximum value of such points is 76.5 dB (about 22 dB below the speaker power). The correlation coefficient in this case was 0.931, indicating a poor array calibration or that the actual source position is not in a grid point. This can also indicate that the source is not a perfect monopole. The time for this computation was just 9.7 s.

The effect of using a finer grid is analyzed in Fig. 17b and is also used to establish the location of the source more accurately. In this case, the grid resolution is 0.5 in. and a detail of the center of the grid is shown. Note that the total level of the source is recovered, in very good agreement with the 1 in. grid resolution case. In this case, artificial sources in the corner of the grid also appeared, with a maximum level of 76.4 dB. The correlation coefficient in this case was 0.937, indicating that the reason for a low correlation is not due to errors induced by missing the actual source position. Because a larger number of grid points are being used, the computational time is increased significantly (i.e., 140 s). In both cases, the number of parameters to optimize was seven. From the previous results, it can be

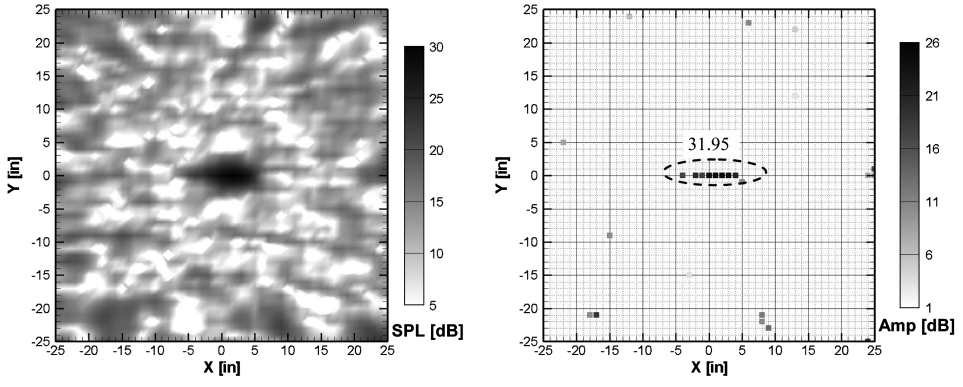

Fig. 13 Plots of a) beamforming simulation for multiple coherent sources with different relative phase at 15 kHz and b) LORE results assuming incoherence.

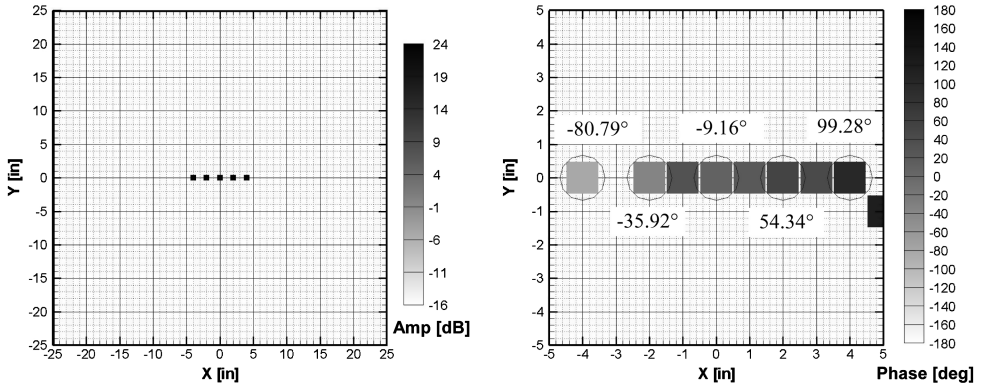

a) b)

Fig. 14 LORE results for multiple coherent sources with different relative phase at 15 kHz: a) amplitude, and b) relative phase (detail).

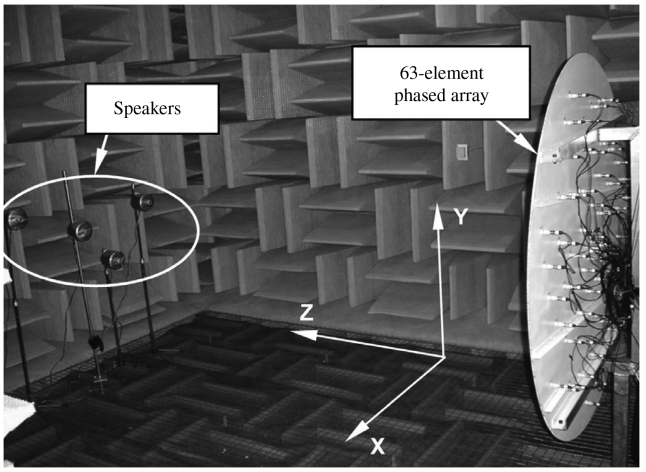

Fig. 15 Test setup for testing LORE capabilities.

concluded that the levels are correctly recovered regardless of grid resolution. That is, the resolution is good enough to identify sources in the beamforming map (e.g., one-third of the beamwidth at the desired frequency). Note that grid resolution also poses a big compromise between computational time and accuracy of the recovered sources position. The required computational resources are also increased because the matrix with the cpsf needs to be allocated in memory.

It is also interesting to see the effect of a bigger scanning grid. In this sense, Fig. 18a shows the beamforming map for a 40 by 40 in. grid with a resolution of 1 in. As can be seen, the side lobes start to appear in the map. The LORE results are presented in Fig. 18b. The recovered level of the source is in good agreement with the previous cases. Note also that there are several artificial sources adding up to 83.7 dB (i.e., about 15 dB below the power of the speaker source). In this case, the correlation coefficient surprisingly dropped to 0.887, indicating that the results should not be considered to be accurate. The time required for this computation was 209 s. This increase in time is related to the increase in grid size and to the number of values to optimize (i.e., 22).

As in the case of numerical simulations, it is very interesting to compare the actual beamforming output with the reconstruction from the LORE results. When dealing with measured data, it is also interesting to compare the previous plots with the theoretical psf for a single source with the same level, thus neglecting the artificial sources.

As can be seen comparing Figs. 19a and 19b, the effect of the artificial sources is to account for the extra side lobes that appear around the main lobe and are not present in the psf (Fig. 19c). The reason for these side lobes in the beamforming output is most likely related to a poor calibration of the array, but it could also be related to the radiation characteristics of the speaker. Note also that the outer side-lobe structure is in relatively good agreement in all cases. It was interesting to find out that (assuming coherence of the sources) the correlation coefficient was 0.993. Thus, the reconstructed beamforming map looked more like the actual map of Fig. 19a, because the artificial lobes are correlated with the speaker.

An important conclusion from this section is that the LORE formulation could be integrated in the calibration procedure so that the array output matches the theoretical psf of the array, thus improving the calibration and LORE results.

It is also interesting to analyze the effect of applying the LORE technique to data beamformed with diagonal removal (DR). Even when the current formulation does not account for DR, the results can still be used to draw some conclusions. Figure 20a shows the beamforming for the same case of a single speaker using the 40 by 40 in. grid. As can be seen, due to the DR processing, the side lobes are significantly reduced. Because the proposed technique is trying to recognize patterns in the beamformed data related to side-lobe levels

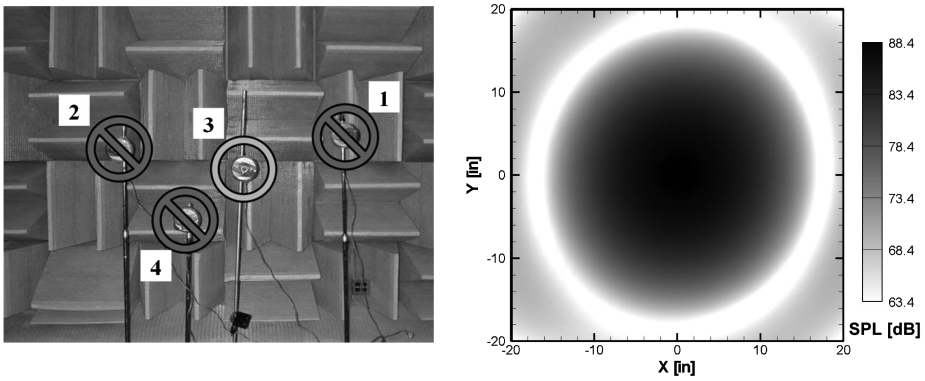

a) b)

Fig. 16 Experimental test with a single source: a) speaker setup and b) beamforming map at 2.2 kHz for a single source.

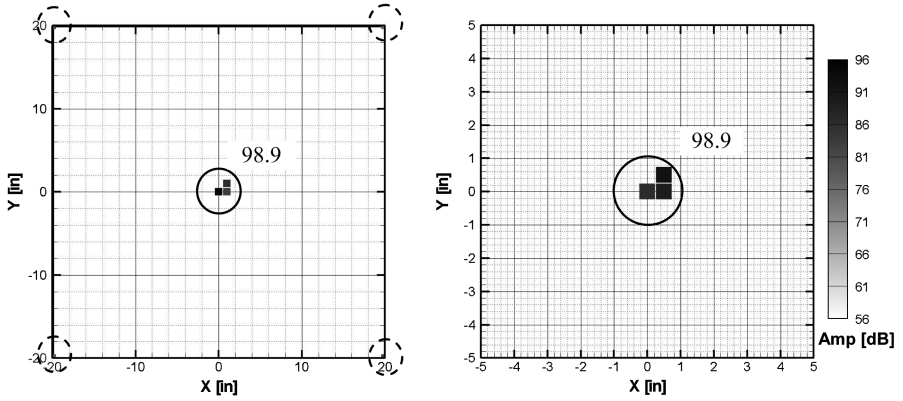

a) b)

Fig. 17 LORE results for a single speaker at 2.2 kHz using a 40 by 40 in. grid with a) 1 in. resolution, and b) $\frac{1}{2}$ in. resolution (detail).

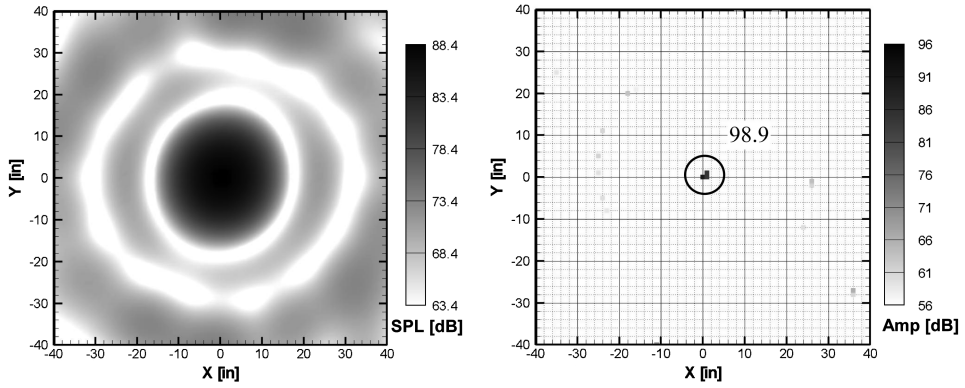

a) b)

Fig. 18 Single speaker at 2.2 kHz using a 80 by 80 in. grid with 1 in. resolution: a) beamforming and b) LORE results (detail).

and locations, some differences are expected to show up in the results. Thus, the main lobe size and levels will be almost the same, but the side-lobe structure will be completely different. A detailed view of the LORE result is shown in Fig. 20b. In this case, the processing rendered only a cluster of three nonzero values at the center of the grid with no artificial sources. The total level recovered for the speaker is 98.7 dB, about 0.2 dB lower than the values recovered without DR on the same grid. This is related to the fact that when diagonal removal is used, power is being removed from the map. Thus, the results obtained when DR is applied are expected to underestimate the actual levels. Because most of the side lobes are not present, the comparison with the reconstruction has significant differences, and thus the correlation coefficient was 0.83. The time required for this computation was only 133 s.

The more complex case of four speakers in the same plane parallel to the array is analyzed next. In this configuration, speakers 1 and 4 were driven with one signal generator, and speakers 2 and 3 were driven with a second signal generator. However, in both cases, the relative phase was adjusted using a phase shifter. The setup and the beamforming map at a frequency of 2.2 KHz are shown in Fig. 21.

The postprocessing results when incoherence is assumed are shown in Fig. 22a. As can be seen, LORE can accurately recover the actual position of the sources. However, a correlation coefficient of 0.75 indicates a lack of accuracy in the results. Assuming coherence, the actual positions of the sources are also accurately recovered, as shown in Fig. 22b. In this case, the correlation coefficient is 0.923, indicating an accurate solution. However, the levels are not in agreement with the expected values (i.e., the level of speaker 2 should be higher and speaker 3 should be the lowest). This difference might be related to an error in the calibration of the speakers' output or a difference in the response of the speakers. Also, LORE is assuming that all sources are coherent and thus not neglecting cross terms

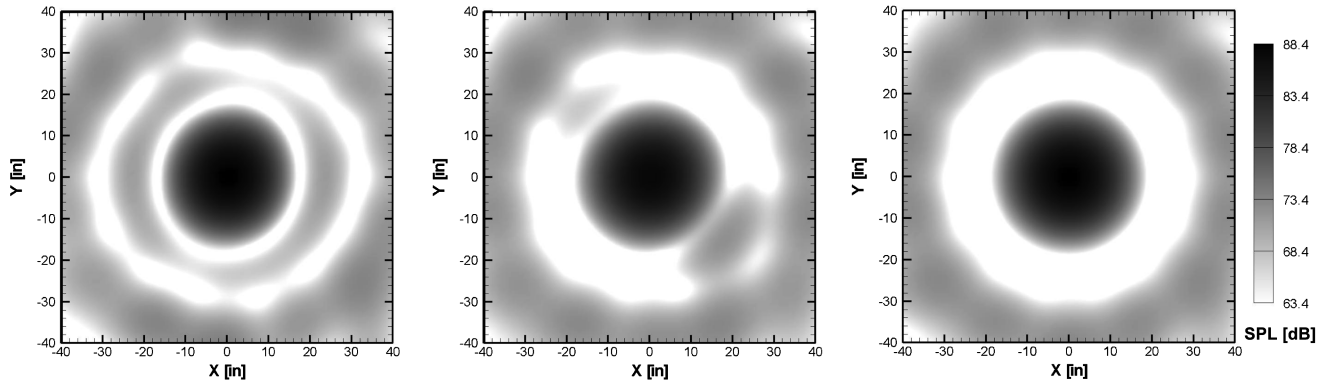

a) b) c)

Fig. 19 Application of LORE to experimental results: a) actual beamforming map, b) reconstruction from LORE results, and c) psf at 2.2 kHz.

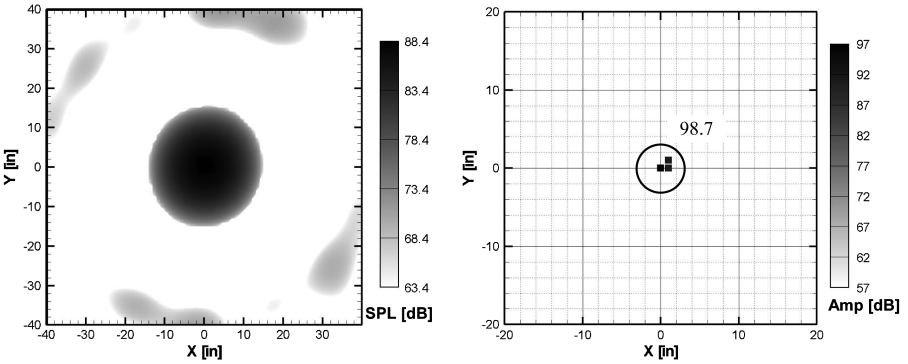

a) b)

Fig. 20 Results for a single speaker using DR beamforming: a) at 2.2 kHz and b) LORE results.

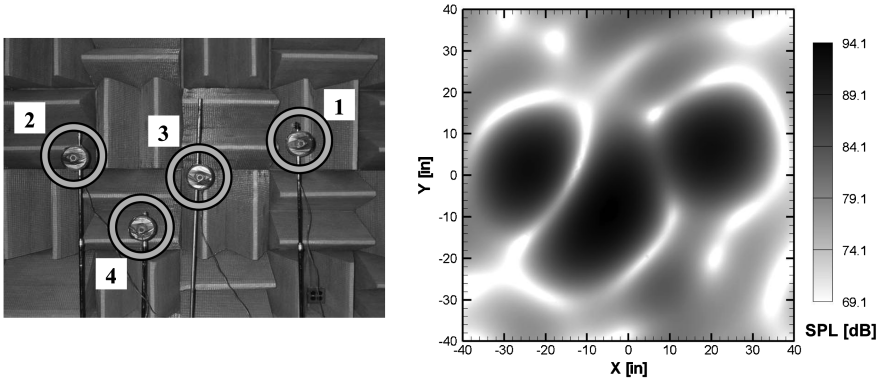

a) b)

Fig. 21 Experimental test with multiple sources: a) speaker setup and b) beamforming map at 2.2 kHz for multiple sources.

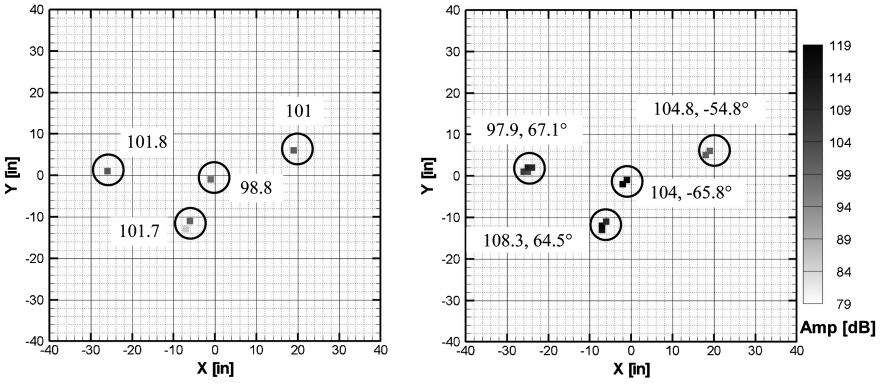

a) b)

Fig. 22 LORE results for four speakers assuming a) incoherent and b) coherent sources.

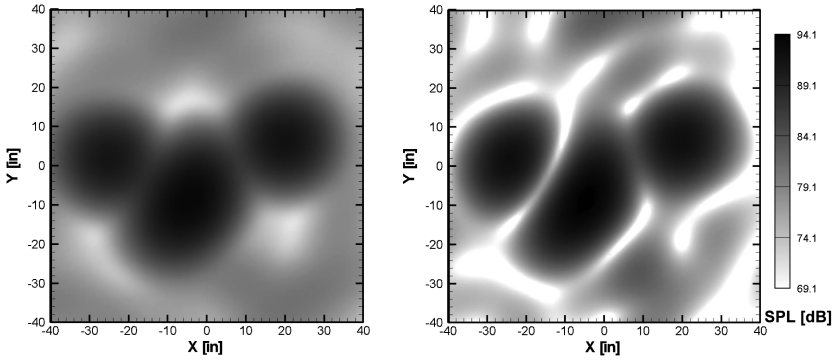

a) b)

Fig. 23 Reconstruction from LORE results for four speakers assuming a) incoherent and b) coherent sources.

between uncorrelated sources. In this case, the approach mentioned before (i.e., using the cross-beamforming) should be used to cancel the correct cross terms and obtain the correct results. The post-processing time for these cases was 127 and 273 s, respectively. In both cases, the number of artificial sources was zero.

The reconstruction for both assumptions is shown in Fig. 23. As can be seen, the reconstruction with the coherence assumption is in very good agreement with the actual beamforming map, whereas the reconstruction from the incoherent results is poor. This suggests that the sources are coherent, in agreement to the experimental setup and the LORE correlation coefficient of 0.923.

VII. Conclusions

Because the analysis of beamforming maps is difficult due to the presence of side lobes and possible coherence between sources, an alternative approach was developed for postprocessing of phased-array measurements. The postprocessing technique is called noise source localization and optimization of phased-array results (LORE). The LORE approach uses a nonlinear model in terms of the sources' amplitudes to accurately model the beamforming output of coherent sources. To this end, the complex point-spread function (cpsf) of the array was defined.

This new approach renders acoustic maps on which only the actual noise sources' positions and their levels are shown (i.e., side lobes are not present). The results from the postprocessing were found to be satisfactory for a wide range of frequencies and source distribution complexity. This includes the case of multiple fully coherent sources, in which the relative phase information was also recovered.

The accurate modeling proposed in this work represents an advance in phased-array postprocessing in terms of reducing computational time and overcoming other limitations reported in currently available approaches (i.e., application being restricted to small regions in space or sources in the boundaries of the scanning grid). It was also proven that even when LORE loses source location accuracy due to poor array resolution at a particular frequency, its results are easier to interpret and more informative than the actual beamforming maps.

The present work represents a first step for LORE in the sense that many features can be implemented to improve the results' accuracy and range of applicability (i.e., the formulation of LORE using diagonal-removal beamforming and the proposed approach of using cross-beamforming to solve partially correlated sources). Also, to improve the accuracy of the results in terms of source location in the presence of several scattered coherent sources, it would be interesting to analyze alternatives to step 1 when coherence is assumed (i.e., a different relaxation of the nonlinear problem).

Experiments with a better calibrated array and speakers should also be performed to further evaluate the capabilities of the proposed approach.

References

[1] Brooks, T. F., and Humphreys, W. M., Jr. "A Deconvolution Approach for the Mapping of Acoustic Sources (DAMAS) Determined from Phased Microphone Arrays," 10th AIAA/CEAS Aeroacoustics Conference and Exhibit, Manchester, England, U.K., AIAA Paper 2004-2954, May 2004.

[2] Brooks, T. F., and Humphreys, W. M., Jr., "Three-Dimensional Application of DAMAS Methodology for Aeroacoustic Noise Source Definition," 11th AIAA/CEAS Aeroacoustics Conference and Exhibit, Monterey, CA, AIAA Paper 2005-2960, May 2005.

[3] Dougherty, R. P., "Extensions of DAMAS and Benefits and Limitations of Deconvolution in Beamforming," 11th AIAA/CEAS Aeroacoustics Conference and Exhibit, Monterey, CA, AIAA Paper 2005-2961, May 2005.

[4] Ehrenfried, K. and Koop, L., "A Comparison of Iterative Deconvolution Algorithms for the Mapping of Acoustic Sources," 12th AIAA/CEAS Aeroacoustics Conference and Exhibit, Cambridge, MA, AIAA Paper 2006-2711, May 2006.

[5] Brooks, T. F., and Humphreys, W. M., Jr., "Extension of DAMAS Phased Array Processing for Spatial Coherence Determination (DAMAS-C)," 12th AIAA/CEAS Aeroacoustics Conference and Exhibit, Cambridge, MA, AIAA Paper 2006-2654, May 2006.

[6] Sijtsma, P., "CLEAN Based on Spatial Source Coherence," 13th AIAA/CEAS Aeroacoustics Conference and Exhibit, Rome, AIAA Paper 2007-3436, May 2007.

[7] Oerlemans, S., and Sijtsma, P., "Determination of Absolute Levels from Phased Array Measurements Using Spatial Source Coherence," 8th AIAA/CEAS Aeroacoustics Conference and Exhibit, Breckenridge, CO, AIAA Paper 2002-2464, June 2002.

[8] Mueller, T. (ed.), *Aeroacoustic Measurements*, Springer, New York, 2002.

[9] Horne, C., Hayes, J. A., Jaeger, S. M., and Srba, J., "Effects of Distributed Source Coherence on the Response of Phased Acoustic Arrays," 6th AIAA/CEAS Aeroacoustics Conference and Exhibit, Lahiana, HI, AIAA Paper 2000-1935, June 2000.

[10] Lawson, C. L., and Hanson, R. J., *Solving Least-Squares Problems*, Prentice–Hall, Englewood Cliffs, NJ, 1974.

[11] Fiacco, A. V., and McCormick, G. P., *Nonlinear Programming: Sequential Unconstrained Minimization Techniques*. Wiley, NY, 1968.

[12] Nelder, J. A., and Mead, R., "A Simplex Method for Function Minimization," *Computer Journal*, Vol. 7, No. 4, 1965, pp. 308–313. doi:10.1093/comjnl/7.4.308

[13] Luersen, M., A., and Riche, R. L., "Globalized Nelder-Mead Method for Engineering Optimization," *Computers and Structures*, Vol. 82, Nos. 23–26, 2004, pp. 2251–2260. doi:10.1016/j.compstruc.2004.03.072

[14] Starck, J. L., Murtagh, F., and Bijaoui, A., "Multiresolution and Astronomical Image Processing," *Astronomical Data Analysis Software and Systems 4*, ASP Conference Series, Vol. 77, edited by R. A. Shaw, H. E. Payne, and J. J. E. Hayes, Astronomical Society of the Pacific, San Francisco, 1995.

[15] *ESO-MIDAS User Manual*, Vol. B, European Southern Observatory, Garching, Germany, 1998.

[16] Starck, J. L., Murtagh, F., and Bijaoui, A., "Multiresolution Support Applied to Image Filtering and Restoration," *Graphical Models and Image Processing*, Vol. 57, No. 5, 1995, pp. 420–431. doi:10.1006/gmip.1995.1036

[17] Lucas, B. D., and Kanade, T., "An Iterative Image Registration Technique with an Application to Stereo Vision," *Proceedings of the Seventh International Joint Conference on Artificial Intelligence*, Aug. 1981, pp. 674–679.

[18] Goshtasby, A., Gage, S. H., and Bartholic, J. F., "A Two-Stage Cross-Correlation Approach to Template Matching," *IEEE Transactions on Pattern Analysis and Machine Intelligence*, Vol. 6, No. 3, 1984, pp. 374–378. doi:10.1109/TPAMI.1984.4767532

J. Wei
Associate Editor